JOURNAL OF AIRCRAFT
Vol. 43, No. 1, January–February 2006

Wing Drag Prediction and Decomposition

D. D. Chao* and C. P. van Dam†
University of California, Davis, Davis, California 95616

A wake integration methodology to predict the aerodynamic characteristics of three-dimensional wings in viscous subsonic and transonic flows is presented. Results indicate that wake integration is viable as a method of drag prediction and, compared to surface integration, has the added benefit of being able to provide a decomposition of the total drag into its physical components of profile, induced, and wave drag for a wing in viscous, transonic flow. Future work will involve using wake integration on postprocess flows about more complex configurations for which this study provides a sound basic framework.

Nomenclature

b	=	wing span
c	=	root chord (reference length)
H	=	total enthalpy
h	=	enthalpy
M_∞	=	freestream Mach number
$\boldsymbol{n}$	=	normal vector
p	=	pressure
q	=	velocity magnitude
R	=	universal gas constant
$\boldsymbol{r}$	=	position vector
s	=	entropy
T	=	temperature
$[\boldsymbol{T}]$	=	stress tensor
U_∞	=	freestream velocity
u^*	=	friction velocity
$\boldsymbol{V}$	=	velocity vector
x, y, z	=	Cartesian coordinates
y^+	=	local Reynolds number, yu^*/ν
α	=	angle of attack
α_i	=	induced angle of attack
Γ	=	total circulation
Λ	=	wing sweep angle
ν	=	kinematic viscosity
ξ	=	x component of vorticity
ρ	=	density
τ	=	viscous stress
ψ	=	stream function

Subscripts

LE	=	leading edge
TE	=	trailing edge
∞	=	freestream conditions

Introduction

THE aerodynamic drag of a transport aircraft flying at transonic speeds can be separated into viscous (or profile) drag, induced drag, and wave drag. Viscous drag consists of skin friction and form drag and is generated through the action of viscosity within the boundary layer. Induced drag is the result of the shedding of vorticity that accompanies the production of lift. Wave drag arises from the radiation of energy away from the aircraft in the form of pressure waves. Accurate prediction of drag during the various stages of the development process of an aircraft is of importance to the efficiency of this process as well as to the economic success of the aircraft. Additionally, knowledge about the physical components of the drag is of importance to the prediction of scale effects on aircraft drag.

The most common technique to calculate the drag of an airfoil, wing, or complete configuration is based on the integration of the pressure and the shear stress acting on the surface of the configuration. An alternative to calculating aerodynamic forces by means of surface integration is to compute the forces around a far-field surface enclosing the body, a technique known as far-field integration. The advantage of this technique is that the shear-stress contribution can be neglected if the control surface is located outside the viscous layer; however, an additional term (momentum flux) must be included in the analysis. A second alternative drag-prediction method is the wake integration technique, which is based on the principle that the aerodynamic drag of a configuration can be obtained from pressure and momentum information in the wake at some distance downstream of the configuration. The main advantage of this technique is that the integration is straightforward and does not require detailed information on the surface geometry of the configuration. It also allows for the decomposition of the drag into its physical components: viscous drag, induced drag, and wave drag.

Both the far-field and wake integration techniques are closely related to the surface integration technique and all three techniques are derived from momentum integral theory. One of the earliest studies on the subject of computational fluid dynamics (CFD)-based drag prediction was by Yu et al,[1] who explored the three different drag prediction techniques for several two- and three-dimensional configurations. Also Slooff and van der Vooren[2,3] as well as Lock[4,5] have published several insightful papers on CFD-based drag prediction. Recently the wake integration technique was successfully applied to the prediction of lift, induced drag, and wave drag of three-dimensional wings in subsonic and transonic flows based on CFD solutions.[6–13] However, most of these studies have been limited to flows governed by the Euler equations. On the experimental side, a good example illustrating the usefulness of wake integration to determine the effect of configuration modifications on drag and its physical components as part of a wind-tunnel experiment is presented by Kusunose et al.[14] The present goal is to apply the wake integration technique to numerical solutions of the three-dimensional Reynolds-averaged Navier–Stokes (RANS) equations for complex configurations.

This paper summarizes the research that has been conducted to attain that ultimate goal and is a continuance of previous studies of two-dimensional drag prediction.[15] The accuracy and consistency of wake integration was first validated through two-dimensional case studies of two single-element airfoils in subsonic and transonic viscous flows.[15,16] The viability of decomposing the drag using wake

Received 18 July 2004; presented as Paper 2004-5074 at the AIAA Applied Aero Conference, Providence, RI, 16–19 August 2004; revision received 1 April 2005; accepted for publication 4 April 2005.

*Graduate Student Researcher, Department of Mechanical and Aeronautical Engineering; currently Aerodynamics Engineer, Cessna Aircraft Company, Wichita, KS.

†Professor, Department of Mechanical and Aeronautical Engineering, One Shields Avenue; cpvandam@ucdavis.edu. Senior Member AIAA.

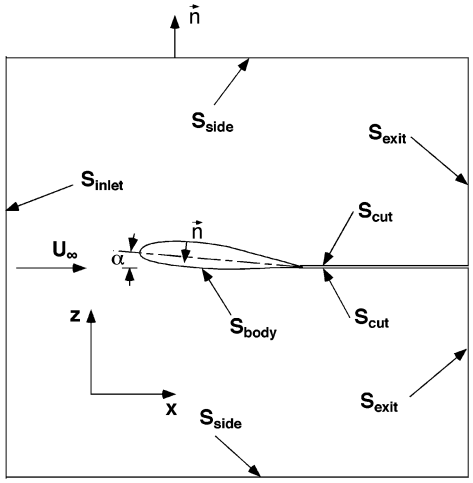

Fig. 1 Control volume used in derivation of aerodynamic forces.

integration was also ascertained in those studies. For this paper, results for three-dimensional, inviscid and viscous flows are presented using a semispan wing with a NACA 0012 profile. Both subsonic and transonic flow conditions are included. This study provides a sound framework for future work involving geometries and grids of ever-increasing complexity.

Force Evaluation Methods

The fundamental formula for the total aerodynamic force acting on a configuration is derived by applying the conservation law of momentum to the control volume enclosing the entire configuration, as shown in Fig. 1. Neglecting body forces, the resulting equation is

$$\int_S [[\boldsymbol{T}] : \boldsymbol{n} - \rho \boldsymbol{V}(\boldsymbol{V}\cdot\boldsymbol{n})]\,\mathrm{d}S = 0 \tag{1}$$

where S represents the entire control surface, $\boldsymbol{n} = n_x\hat{\boldsymbol{i}} + n_y\hat{\boldsymbol{j}} + n_z\hat{\boldsymbol{k}}$ represents the outward unit vector normal to S, ρ represents the fluid density, and $\boldsymbol{V} = u\hat{\boldsymbol{i}} + v\hat{\boldsymbol{j}} + w\hat{\boldsymbol{k}}$ represents the velocity vector.

The tensor product $[\boldsymbol{T}] : \boldsymbol{n}$ contains contributions from the pressure p and the viscous stress τ. The aerodynamic drag, defined as the force in the freestream direction imposed by the fluid on the configuration, is

$$D = -\int_{S_{\text{body}}} [-pn_x + \tau_{xx}n_x + \tau_{xy}n_y + \tau_{xz}n_z]\,\mathrm{d}S \tag{2}$$

or

$$D = \int_{S_{\text{far}}} [-pn_x + \tau_{xx}n_x + \tau_{xy}n_y + \tau_{xz}n_z - \rho u(\boldsymbol{V}\cdot\boldsymbol{n})]\,\mathrm{d}S \tag{3}$$

where the freestream velocity vector is aligned with the x axis (Fig. 1). Equations (2) and (3) represent the surface, or near-field, and far-field expressions for the drag, respectively. To correct for any mass conservation error in the flowfield, the far-field expression can be evaluated as follows:

$$D = \int_{S_{\text{far}}} [-pn_x + \tau_{xx}n_x + \tau_{xy}n_y + \tau_{xz}n_z - \rho(u - U_\infty)(\boldsymbol{V}\cdot\boldsymbol{n})]\,\mathrm{d}S \tag{4}$$

where U_∞ represents the freestream velocity. The exit-plane expression for the drag can be derived from Eq. (4) by moving the inlet and side faces to infinity. The resulting expression is

$$D = \int_{S_{\text{exit}}} [(p_\infty - p) + \tau_{xx} - \rho u(u - U_\infty)]\,\mathrm{d}S \tag{5}$$

where S_{exit} is normal to the freestream velocity vector, which again is aligned with the x axis.

Equations (2), (4), and (5), presented here in their most general form, provide three fundamental integrals for the evaluation of the aerodynamic drag. Note that these three expressions should predict an identical drag value for any given flowfield. However, as a result of problems encountered in the numerical integration of these expressions as well as various errors and limitations contained in the discrete nature of numerical flow solutions, the drag values may differ substantially. Surface integration is used because it is the most common form of drag evaluation and corresponds to the force-balance method used in experimental force measurements. The far-field formulation is similar to the surface integration except with the additional advantage of specifying the integration surface without necessarily having to follow the geometric details of the configuration. The viscous stresses can also be neglected if the far-field integration surface is selected far enough away from the configuration. In this paper, however, the far-field formulation is not evaluated because it similarly offers no exceptional insights into the sources of drag production compared to surface integration and is less commonly applied. The exit-plane formulation is used because one main objective is to evaluate the accuracy and consistency of the wake analysis method, and this methodology corresponds to the wake-traverse method that is being increasingly used in experimental force calculations.

Assuming that the contribution of the τ_{xx} viscous stress in the wake is negligible (see Ref. 13 for a detailed discussion of this assumption), Eq. (5) can be expressed in terms of the gradients of the flow variables on the exit plane S_{exit}. Introducing the position vector $\boldsymbol{r} = y\hat{\boldsymbol{j}} + z\hat{\boldsymbol{k}}$ and noting that all flow variables approach their freestream values at the edge of the infinite plane, it can be shown that

$$D = \frac{1}{2}\iint_{S_{\text{exit}}} [(\boldsymbol{r}\cdot\boldsymbol{\nabla})(p + \rho u^2)]\,\mathrm{d}S \tag{6}$$

In this gradient form it is possible to decompose the drag into its physical components. Using the magnitude of the velocity vector, $q^2 = \boldsymbol{V}\cdot\boldsymbol{V}$, and the combined first and second laws of thermodynamics, $\boldsymbol{\nabla} p = \rho\boldsymbol{\nabla} h - \rho T\boldsymbol{\nabla} s$, Eq. (6) can be written as follows:

$$D = \frac{1}{2}\iint_{S_{\text{exit}}} \left\{\boldsymbol{r}\cdot\left[\rho\boldsymbol{\nabla}\left(h + \frac{1}{2}q^2\right) - \rho T\boldsymbol{\nabla} s - \frac{1}{2}\rho\boldsymbol{\nabla}(v^2 + w^2 - u^2) + u^2\boldsymbol{\nabla}\rho\right]\right\}\mathrm{d}S \tag{7}$$

The first term in Eq. (7) involves the total enthalpy term, $H = h + \frac{1}{2}q^2$. To a close approximation the expression for the drag can now be written as[13]

$$D = -\rho_\infty \iint_{S_{\text{wake}}} \Delta H + \frac{p_\infty}{R}\iint_{S_{\text{wake}}} \Delta s\,\mathrm{d}S + \frac{\rho_\infty}{2}\iint_{S_{wake}} (\psi\xi)\,\mathrm{d}S \tag{8}$$

where the variable ψ is a scalar function for the crossflow velocities and ξ is the x component of the vorticity vector as proposed by Maskell.[17] Equation (8) represents the wake-integral formulation of the drag. Limiting application to configurations with the propulsion system switched off and with adiabatic surfaces, the contribution of the first integral in Eq. (8) becomes negligible and the resultant well-known expression for the drag is

$$D = \frac{p_\infty}{R}\iint_{S_{\text{wake}}} \Delta s\,\mathrm{d}S + \frac{\rho_\infty}{2}\iint_{S_{\text{wake}}} (\psi\xi)\,\mathrm{d}S \tag{9}$$

where the first integral represents the sum of the viscous drag and the wave drag, and the second integral represents the induced drag. The former integral should be evaluated across the shocks to obtain only the wave-drag contribution. A second reason to limit this integration to the flow region containing the shocks is to minimize the influence

of spurious entropy (present in most if not all flowfield simulations based on the Euler or Navier–Stokes equations) on the wave drag. The second integral represents the vortex or induced drag, which accompanies flows over wings of finite span. The benefit of this formulation is that both integrals need only be integrated across the wake region and not the entire exit plane. Another benefit is that the mechanisms by which the total drag may be decomposed can be readily seen and understood.

The lift can also be evaluated using the two techniques of surface integration and wake integration. For surface integration, the formulation is given by

$$L = -\int_{S_{\text{body}}} [-pn_z + \tau_{zx}n_x + \tau_{zy}n_y + \tau_{zz}n_z]\,\mathrm{d}S \tag{10}$$

Using Maskell's[17] formulation, the lift can also be evaluated from the wake area and the final form is presented here:

$$L = \rho_\infty U_\infty \int_{S_{\text{wake}}} y\xi\,\mathrm{d}S \tag{11}$$

As stated before, although wake integration and surface integration should ideally produce the same values for lift and drag, numerical approximations may render the actual results quite differently.

Numerical Implementation

For the analysis, a postprocessor incorporating the wake integral method for lift and drag has been developed. Three-dimensional surface integration is performed using the FOMOCO toolset as described under the OVERFLOW solver in the next section.[18,19] For wake integration, the x location for a wake plane downstream of the configuration is first specified. The y and z coordinates are then distributed across this integration plane such that the points cluster near the wing tip to adequately capture the vortex core in this region. The advantage is that any type of integration plane can be specified without being limited to the grid type used for the original solution. Trilinear interpolation is used to interpolate the primitive variables from surrounding grid points onto the wake integration plane.

Flow Solver and Grid Generator

Computations were conducted with OVERFLOW, a three-dimensional compressible RANS flow solver developed by Buning et al. at NASA.[18] Steady and time-accurate solutions can be calculated on structured block or Chimera overset grids. OVERFLOW includes several turbulence models and incorporates various numerical schemes developed from previous research codes such as ARC2D[20] as well as other earlier flow solvers. Various zero-, one-, and two-equation turbulence models are available in OVERFLOW. However, because the objective of this study is not a comparison of the different turbulence models but a comparison of drag prediction techniques, the Spalart–Allmaras model[21] was selected and used throughout the three-dimensional study. Another feature of OVERFLOW is the inclusion of a low-Mach preconditioning algorithm for improved convergence and solution quality at low Mach numbers.[22] The necessity of this feature will be detailed in the results section, but its integration into this flow solver simplifies the accurate comparison of its effects, because only this parameter and nothing else need be varied for the same flow conditions.

OVERFLOW also comes with the postprocessing FOMOCO toolset.[19] This toolset calculates the lift and drag coefficients using surface integration and is composed of two programs, MIXSUR and OVERINT. MIXSUR processes the original overset mesh configuration and forms body surface grids as specified by the user. Integration of values is then performed using the OVERINT program to calculate all surface forces and moments.

For this study, a single C-H grid is used to cover a semispan wing (Fig. 2). For the inviscid cases, in both the leading-edge and the trailing-edge regions, the initial circumferential grid spacings are set at 1×10^{-4}, and the initial wall spacing is set at 1×10^{-4}. Final mesh size is approximately 3 million grid points. For the viscous cases, the initial circumferential spacings remain at 1×10^{-4} for both the leading-edge and the trailing-edge regions. Wall spacing, however, is reduced to 1×10^{-6} for $y^+ < 1$. Final mesh size is on the order of 6 million grid points. For all cases, the far field is located approximately 50 root chords away, and the angle of attack is set at $\alpha = 4$.

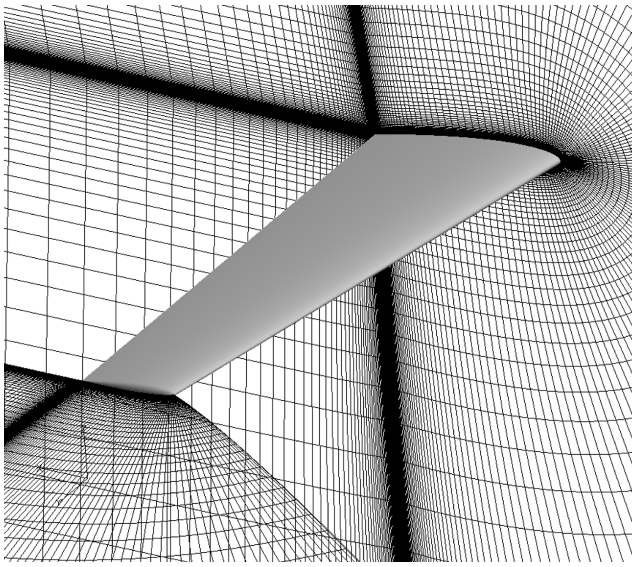

Fig. 2 Sample grid for baseline NACA 0012 wing.

Baseline Wing

For the wing, a NACA 0012 profile is used. The taper ratio is 0.5 with the root chord representing the reference length. The straight trailing edge is unswept and the leading edge is allowed to sweep as necessary to meet the linear taper. The nominal span is 5.25, resulting in a wing aspect ratio of 7. This span value does not include the rounded wing cap and so the actual span is slightly greater. For all subsonic cases, the freestream Mach number is 0.25 with a Reynolds number of 1.0×10^6. For the transonic cases, the Reynolds number remains unchanged, but the freestream Mach number is increased to 0.73 for both the inviscid case as well as for the viscous case. Full turbulence is specified for the viscous cases to avoid boundary-layer transition issues.

Results and Discussion

For all cases, the OVERFLOW solution is run in steady-state mode with central differencing on the right-hand side and ARC3D three-factor block tridiagonal scheme on the left-hand side.[18] Second- and fourth-order dissipation values are kept at 0.0 and 0.02, respectively, for the subsonic cases and 2.0 and 0.04, respectively, for the transonic cases.[18] Solutions are deemed converged when residuals are reduced to effectively machine zero, and the surface lift and drag coefficients are converged to within ± 0.0001 and ± 0.00001 (± 0.1 drag count), respectively.

Inviscid Flow

For the inviscid subsonic case, lift as calculated from surface integration gives a coefficient value of 0.350. Using a wake analysis position one root chord aft of the wing, wake integration gives a lift coefficient of 0.352. These two values compare very well with each other. For the transonic case, surface integration predicts a lift coefficient of 0.462, and wake integration predicts 0.463. These values indicate that lift prediction is consistent between the two lift-prediction methods.

Establishing the position of the wake integration plane one root chord downstream of the wing as opposed to five or ten chords was done to emulate likely wind-tunnel conditions. In most wind-tunnel experiments, the wake traverse is conducted close to the configuration because space in the test section tends to be limited. Also, wake positions of less than one root chord are not used because the viscous

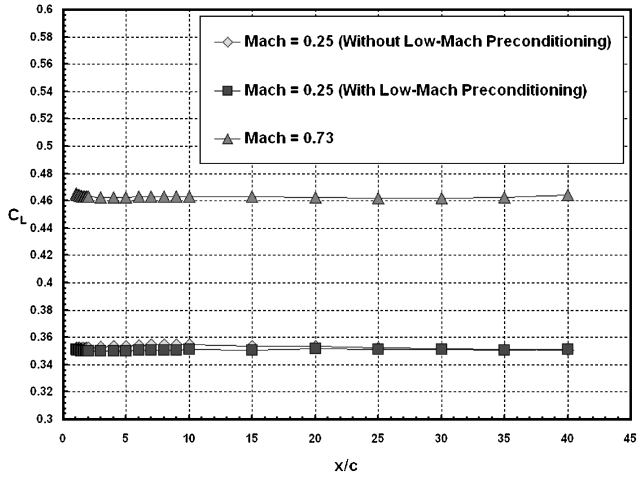

Fig. 3 Consistency of lift coefficient downstream of wing for inviscid flow cases.

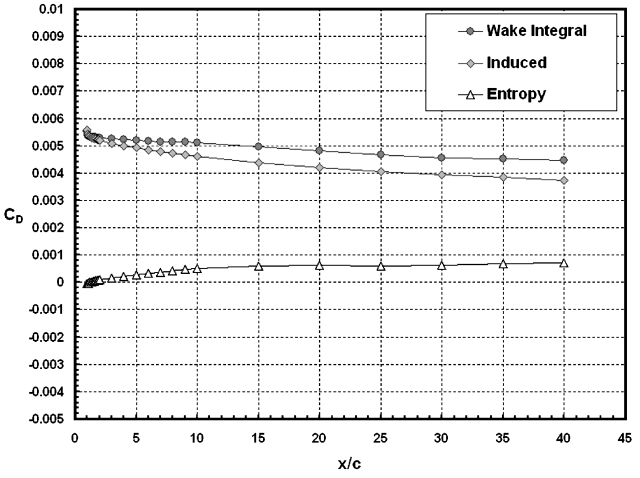

Fig. 4 Consistency of wake integration downstream of wing for inviscid, subsonic flow without low-Mach preconditioning ($M_\infty = 0.25$).

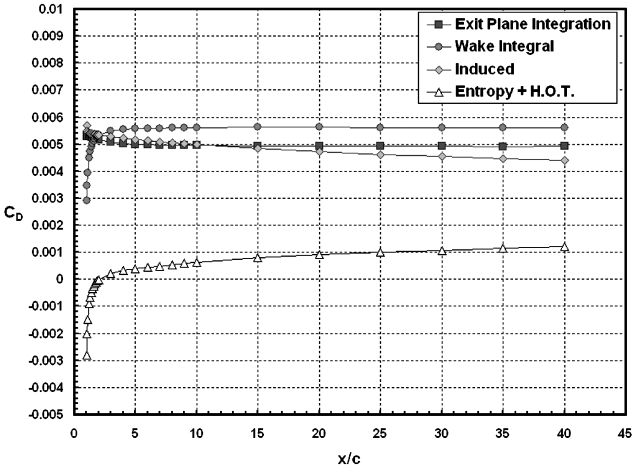

Fig. 5 Consistency of wake integration downstream of wing for inviscid, subsonic flow with low-Mach preconditioning ($M_\infty = 0.25$).

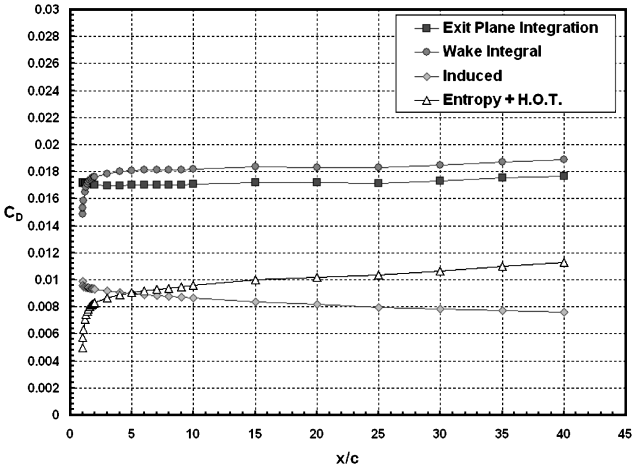

Fig. 6 Consistency of wake integration downstream of wing for inviscid, transonic flow ($M_\infty = 0.73$).

term τ_{xx} is not accounted for in the final wake integral formulation used here and in experimental wake studies, and effects in the near wake are not well resolved using the thin-layer approximation in the numerical flow solution. Another reason (discussed in more detail later) is that, under the influence of viscosity (numerical as well as physical), induced drag slowly decreases with increasing downstream distance and this decrease in drag is balanced by a gradual increase in entropy drag. Selecting a wake position of one root chord aft of the wing preserves the nominal value of the induced drag.

The lift development downstream from the wing for the subsonic and transonic cases is depicted in Fig. 3. For all three conditions, the lift is nearly constant downstream of the wing, as expected. For the subsonic flow ($M_\infty = 0.25$), a separate case using low-Mach preconditioning is also analyzed for comparison. The lift behavior with preconditioning is slightly more consistent than lift development without preconditioning, but nothing indicates that preconditioning is necessary under these low-Mach-number conditions.

The drag coefficients for the subsonic case are 0.0058 from surface integration and 0.0056 from wake integration based, again, on a wake analysis position of one root chord downstream of the wing. As an additional comparison, the drag using Eq. (5) (exit-plane integral) is calculated to be 0.0050. These drag values are fairly consistent except for the exit-plane formulation, which underpredicts the drag. The latter formulation is expected to underpredict the drag because the integral should be evaluated over the entire, infinite exit plane, whereas the computational domain is limited to about 100 by 50 root chords.

For the transonic case, surface integration predicts a drag coefficient of 0.0170, wake integration a value of 0.0176, and the exit-plane formulation a drag coefficient value of 0.0170. Again, these are fairly consistent results, except that the wake integral formulation overpredicts the drag. This is likely due to the contribution of a certain amount of spurious entropy. This influence will be discussed later when the tabulated results are summarized.

Drag development in the wake is illustrated in Figs. 4 and 5 for the subsonic case and in Fig. 6 for the transonic case. For the subsonic case (see Fig. 4), the total drag does not remain constant moving downstream. In fact, the total drag drops by some 10 drag counts from the near wake to the far wake. This discrepancy was judged to be too large to be due to loss of grid resolution marching away from the wing. Analysis of the wake revealed that the crossflow velocity components are an order of magnitude less than the freestream Mach number. These crossflow components dissipated further marching downstream of the wing. To resolve this, the low-Mach preconditioning algorithm in OVERFLOW was switched on, and its effect on the wake drag can be observed in Fig. 5. Clearly, the low-Mach preconditioning has greatly improved the consistency of the drag. The total drag is now nearly constant as expected except for the very near wake. As a further check, drag from integrating the exit plane as calculated using Eq. (5) is also evaluated for this case. Except for the very near wake, this integral produces drag values that are consistently lower than wake integration [Eq. (9)] by some six drag counts but otherwise follow the same trend. The largest effect from preconditioning can be seen in the wake behavior of the induced drag. With low-Mach preconditioning, there is still a gradual decrease in the induced drag, which is expected, but the rate of decrease is noticeably less severe compared to the same case without preconditioning. This is consistent with the preceding observation

that the crossflow kinetic energy was dissipating too quickly without low-Mach preconditioning.

Figures 4 and 5 point toward surveying the drag development in the wake as an additional indication of the need for utilizing low-Mach preconditioning. This is especially important because a freestream Mach number of 0.25 usually does not trigger much concern about low-Mach effects on solution convergence and accuracy. Typically, such concerns only come to the fore when the Mach number drops to 0.15 or lower. By only analyzing surface data, the results do not disprove the conventional acceptance. Residuals and lift and drag from surface integration can appear to indicate that the solution is converged, but wake analysis can prove the flowfield is still not fully developed.

For the very near wake, the noticeable dip in the wake total drag in Fig. 5 compared to Fig. 4 is due to the inclusion of a higher-order term in the drag calculations. This was done because this should provide better consistency between drag values calculated from the exit-plane integral [Eq. (5)] and from wake integration [Eq. (9)]. This is because, in deriving Eq. (9), certain higher-order terms are parsed from the full equation given by Eq. (5) and then commonly neglected. Research in two-dimensional wake integral drag prediction suggests these higher-order terms can be quite significant especially in the very near wake.[16] Including this higher-order term, the wake total integration is now given by

$$D = \frac{p_\infty}{R}\iint_{S_{\text{wake}}} \Delta s \, \mathrm{d}S + \frac{\rho_\infty}{2}\iint_{S_{\text{wake}}} (\psi\xi)\, \mathrm{d}S$$

$$- \frac{\rho_\infty}{2}\left(1 - M_\infty^2\right)\iint_{S_{\text{wake}}} (\Delta u)^2 \, \mathrm{d}S \tag{12}$$

and this equation will be used for all further wake integral drag calculations. The inclusion or exclusion of the higher-order term does not impact the drag consistency in the far wake, because the higher-order term reduces to zero marching away from the wing. Thus, the improved consistency of the drag shown in Fig. 5 is solely due to preconditioning.

For the inviscid transonic case (Fig. 6), the total drag from both wake integral and wake total integration is nearly constant downstream of the wing. Just as for the subsonic case, drag from exit-plane integration compared to wake integration is lower, differing by up to 10 drag counts in the far wake, but shows better consistency in the near wake. Again, the total drag from wake integration shows a noticeable dip in the near wake.

As is more clearly illustrated here, use of numerical viscosity has the effect of converting trailing vorticity into entropy. Consequently, as the induced drag decreases, the entropy drag increases, but the total drag essentially remains the same except for the very near field and the very far field. Poorer grid resolution relative to the near field (due to increasingly larger, stretched cells with higher, skewed aspect ratios marching away from the wing) results in the generation of more false entropy in the far field. This, as well as effects from real entropy due to shock formation, likely accounts for the gradual increase in the total drag downstream of the wing.

Figure 7 depicts the spanwise load distribution for the wing in transonic flow compared to the ideal elliptical load distribution. According to linear lifting-line theory, the elliptical load distribution is ideal because it produces the minimum amount of induced drag for a planar wing. The area under this curve is always unity, facilitating the comparison of the various load distributions with the elliptic loading. Both the spanwise load distribution for the wing using the baseline or reference wing geometry values (without the wing cap) and the distribution using the true geometry values (including the wing cap) show a slight spike near the tip. This spike is the result of trailing wake roll-up. This effect is not modeled in lifting-line theory, and, hence, there is a discrepancy near the tip. Both curves agree well with the elliptic distribution, which is indicative of the fact that the induced drag should be near minimum.

For the inviscid cases, the lift and drag values are summarized in Tables 1 and 2. Because no experimental data exist for this specific wing configuration, these results only evaluate the consistency between the surface integral predictions and the wake integral predictions. All wake values are evaluated one root chord aft of the wing. For the lift coefficient, excellent agreement is achieved between surface integration and wake integration for both cases. For the drag coefficient, overall results are very good. For the subsonic case, surface integration and wake total integration [using Eq. (9)] predict almost the same drag value, differing by two drag counts. As a further check for consistency, drag from exit-plane integration [using Eq. (5)] is also used. Although this formulation underpredicts the drag by about six to eight drag counts compared to both surface integration and wake integration, this is still a fairly good result. For the induced drag, linear theory (Prandtl's lifting-line theory) is also applied and compared to the numerical wake prediction. In this case, the induced drag is evaluated based on the spanwise load distribution as illustrated in Fig. 7. The induced drag equation from lifting-line theory is given as

$$D_i = \rho_\infty U_\infty \int_{-b/2}^{b/2} \Gamma(y_0)\alpha_i(y_0)\, \mathrm{d}y_0 \tag{13}$$

Table 1 Inviscid results for NACA 0012 wing

Evaluation method	Subsonic, $M_\infty = 0.25$	Transonic, $M_\infty = 0.73$
Lift: surface, Eq. (10)	0.350	0.462
Lift: wake, Eq. (11)	0.352	0.463
Drag: surface, Eq. (2)	0.0058	0.0170
Drag: exit, Eq. (5)	0.0050	0.0170
Drag: wake, Eq. (9)	0.0056	0.0176
Induced	0.0052	0.0093
Wake entropy	0.0004	0.0083
Drag: induced, Eq. (13)	0.0057	0.0095
Drag: wave	n/a	0.0080

Table 2 Effects of low-Mach preconditioning on inviscid, subsonic test case ($M_\infty = 0.25$)

Evaluation method	No low-M preconditiong	With low-M preconditiong
lift: surface, Eq. (10)	0.350	0.349
Lift: wake, Eq. (11)	0.352	0.350
Drag: surface, Eq. (2)	0.0058	0.0056
Drag: exit, Eq. (5)	0.0050	0.0052
Drag: wake, Eq. (9)	0.0056	0.0056
Induced	0.0052	0.0053
Wake entropy	0.0004	0.0003
Drag: induced, Eq. (13)	0.0057	0.0056

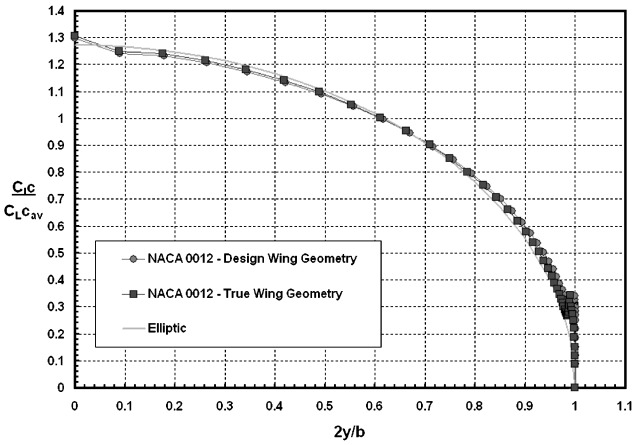

Fig. 7 Spanwise load distribution based on surface integration for inviscid transonic case ($M_\infty = 0.73$).

where Γ is the sectional circulation, b is the wing span, and α_i is the local induced angle of attack given by

$$\alpha_i(y_0) = -\frac{1}{4\pi U_\infty}\int_{-b/2}^{b/2}\frac{\mathrm{d}\Gamma(y)/\mathrm{d}y}{y_0 - y}\,\mathrm{d}y \tag{14}$$

Caution should be exercised when comparing theory to the numerical data, because the theory is a linear simplification of the actual flow. In cases where flow separation or strong spanwise flow exists on the wing, linear theory breaks down. However, the cases studied here exhibit neither condition. Linear theory overpredicts the induced drag by about five drag counts compared to wake integration. However, the linear theory value is essentially the same as the wake total integration value. For this inviscid, subsonic case, ideally, the total drag is only due to the induced drag. However, some false entropy is inevitably generated under these conditions because of the need for artificial viscosity to stabilize the solution. This artificial viscosity also has the effect of converting some trailing vorticity into entropy. Thus, comparing the induced drag from linear theory to the total wake integration value is not inconsistent.

For the transonic case, excellent agreement is achieved between surface integration and wake integration. Wake integration overpredicts the drag by about six drag counts. This is likely due to the fact that, for this case, a real shock exists producing real entropy, which necessitates an increase in the numerical viscosity. This, however, tends to increase the amount of false entropy generated in the wake as well.

Ideally, in the wake, the entropy should only be due to that generated by the shock. By isolating the shock, the wave drag can be calculated. This wave drag value is three drag counts lower than that obtained from integrating the wake entropy. This indicates that a small amount of spurious entropy is generated and captured by the wake integral technique. Also, a small amount of spurious entropy could be contaminating the wave-drag calculations as well, although this would be difficult to quantify. Adding this wave-drag value to the wake-induced drag results in a total drag value of 173 drag counts, which is slightly more consistent with both surface integration and wake integration. For the induced drag, linear theory calculates a value two drag counts higher than wake-induced integration. These results indicate that wake integration is fairly consistent with surface integration. These results also indicate that wake integration can be viably used to decompose the total drag into its physical components.

Table 2 shows the effects of low-Mach preconditioning on the subsonic case using the same wake station for the wake analysis techniques. Compared to the same case before with no preconditioning applied, the effects are rather subtle. For a Mach number of 0.25, preconditioning is usually not mandated and the results in Table 2 support this assumption. Convergence and accuracy at this Mach number are not commonly noted problem issues, especially when looking only at the surface data. However, only through examination of the wake behavior as shown in Figs. 4 and 5 does it become clear that preconditioning is necessary to fully converge the wake to the proper state.

Viscous Flow

For the viscous, subsonic case (see Table 3), the lift coefficient calculated from surface integration is 0.323 compared to 0.325 from wake integration. For the transonic case, surface integration predicts a lift coefficient of 0.413 compared to 0.416 from wake integration. Again, similar to the inviscid cases, the lift values are very consistent between the two lift prediction formulations.

Figure 8 charts the lift development in the wake downstream of the wing. All three cases exhibit great consistency throughout the wake. For the two subsonic cases, low-Mach preconditioning has negligible effect on the lift.

From Table 3, for the drag coefficient values, surface integration predicts a coefficient of 0.0150 for the subsonic case and 0.0242 for the transonic case. Wake integration predicts 0.0152 for the subsonic case and 0.0246 for the transonic case. Exit-plane integration calculates a drag coefficient of 0.0148 for the subsonic case and a coefficient of 0.0243 for the transonic case. For both the subsonic and transonic cases, these drag values are in very close agreement.

Table 3 Viscous results for NACA 0012 wing

Evaluation method	Subsonic, $M_\infty = 0.25$	Transonic, $M_\infty = 0.73$
Lift: surface, Eq. (10)	0.323	0.413
Lift: wake, Eq. (11)	0.325	0.416
Drag: surface, Eq. (2)	0.0150	0.0242
Drag: exit, Eq. (5)	0.0148	0.0243
Drag: wake, Eq. (12)	0.0152	0.0246
Induced	0.0045	0.0075
Wake entropy	0.0107	0.0171
Drag: induced, Eq. (13)	0.0046	0.0074
Drag: wave	n/a	0.0055

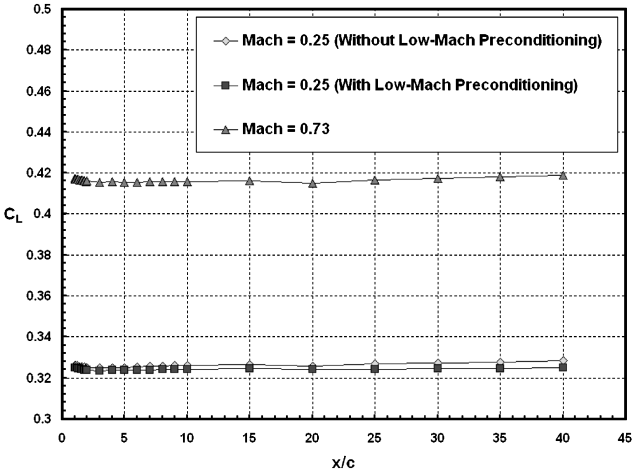

Fig. 8 Consistency of lift coefficient downstream of wing for viscous flow cases.

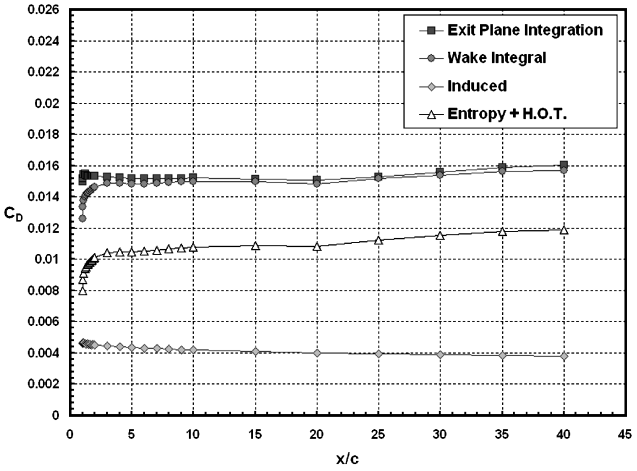

Fig. 9 Consistency of wake integration downstream of wing for viscous, subsonic flow without low-Mach preconditioning ($M_\infty = 0.25$).

The consistency of the drag development downstream of the wing can be observed from Figs. 9 and 10 for the subsonic case and from Fig. 11 for the transonic case. For the subsonic case without low-Mach preconditioning (Fig. 9), the consistency of the drag as calculated from wake integration and exit-plane integration is fairly good out to a far-field distance of approximately 20 root chords aft of the wing. From there, the drag increases as calculated from both formulations.

For the same case but with low-Mach preconditioning, an improvement to the consistency of the drag, especially in the far field, can be readily observed (Fig. 10). The drag is now fairly constant out to approximately 30 root chords aft of the wing before increasing

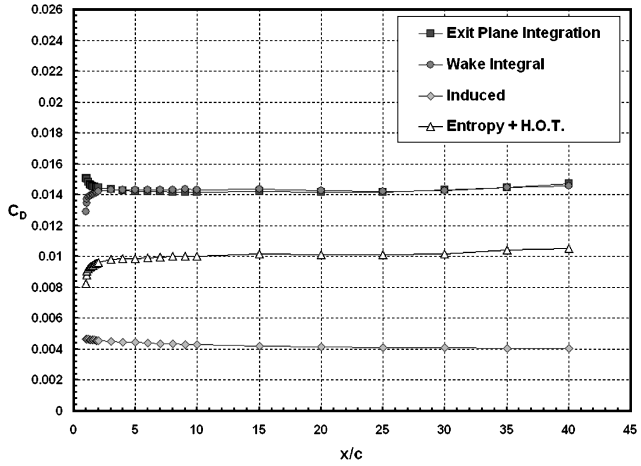

Fig. 10 Consistency of wake integration downstream of wing for viscous, subsonic flow with low-Mach preconditioning ($M_\infty = 0.25$).

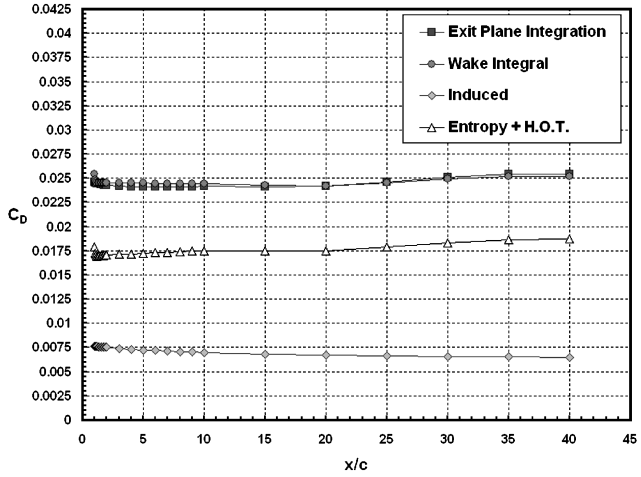

Fig. 11 Consistency of wake integration downstream of wing for viscous, transonic flow ($M_\infty = 0.73$).

steadily. The main effect of preconditioning is seen in the entropy, which is consistently lower at every wake station compared to the case without preconditioning. Even for the near field, the consistency of the drag has been further improved. From this, although preconditioning is arguably not necessary for the viscous subsonic case, it clearly does offer benefits to wake analysis techniques.

For the transonic wake drag shown in Fig. 11, again good consistency is maintained out to a far field of approximately 20 root chords before increasing. In general, the same trends observed for the preceding cases apply here as well. For this case, agreement between wake integration and exit-plane integration is excellent. What is especially noteworthy for this case is the excellent agreement between wake integration drag and exit-plane integration drag in the very near wake. This appears to indicate that the flow solver might be optimized overall for viscous transonic flow, and deviations from this condition may introduce simplifications and approximations that result in discrepancies in the near field. As stated before, a higher-order drag term has been included in these calculations. Without this term, discrepancies in drag between wake integral and exit-plane integration would be significantly larger.

For all the viscous cases, the lift and drag values are summarized in Tables 3 and 4. Again the comparison only evaluates the consistency between the prediction methods. For the lift coefficient, surface integration and wake integration show excellent agreement for both cases. For the drag coefficient, just as for the inviscid cases, overall results are very good. For the subsonic case, good agreement is obtained between surface integration and both wake integration formulations. Using linear theory, the induced-drag values match up

Table 4 Effects of low-Mach preconditioning on viscous, subsonic test case ($M_\infty = 0.25$)

Evaluation method	No low-M preconditioning	With low-M preconditioning
Lift: surface, Eq. (10)	0.323	0.322
Lift: wake, Eq. (11)	0.325	0.324
Drag: surface, Eq. (2)	0.0150	0.0150
Drag: exit, Eq. (5)	0.0148	0.0150
Drag: wake, Eq. (12)	0.0152	0.0153
Induced	0.0045	0.0046
Wake entropy	0.0107	0.0107
Drag: induced, Eq. (13)	0.0046	0.0045

quite well. For the transonic case, better consistency is seen between the two wake integration formulations than with surface integration, but the results are still acceptable. Again, for the induced drag, great consistency is maintained between wake integration and linear theory. Because the flow is viscous, the wake entropy contains entropy generated from real viscosity as well as from any shocks; thus, the wake entropy drag now contains both viscous drag and wave drag.

However, as was done for the inviscid transonic case, the shock is still isolated using a parameter based on the pressure gradient similar to the one developed by Paparone and Tognaccini.[12] This parameter acts as a limiter to isolate the "inviscid" portion of the shock. Entropy generated from viscosity is orders of magnitude larger than the entropy generated from the shock; thus, even minor contamination from viscous entropy can greatly skew the wave-drag results. However, the complete shock extends into the boundary layer, but separating the effects of the shock from the effects of the boundary layer is not possible at this point until the physics of their interaction is better understood. For now, isolating the shock really means isolating that portion of the shock that will produce the equivalent wave-drag value. This complicates the separation of profile drag from wave drag, but other studies[12,15] prove this is within reason. Therefore, even for the viscous cases, wake integration has been shown to be a viable drag prediction method. More significantly, wake integration still retains the benefits of drag decomposition.

Low-Mach preconditioning is also applied to the viscous subsonic case and the results are tabulated and compared to the original case in Table 4. Similar to the inviscid comparison, effects of low-Mach preconditioning are not notably significant. Analysis of only the surface information hardly yields any noticeable differences. The wake data show minor differences but nothing suggests preconditioning gives commandingly better results. As discussed before, the effects of preconditioning on the flowfield solution are only fully understood by examining the development of the drag downstream of the wing through wake analysis techniques as illustrated in Figs. 9 and 10.

Design Test Cases

To further emphasize the utility of using wake integration to decompose the total drag, additional cases using a slightly modified wing are analyzed for comparison to the baseline wing. The baseline wing has a trailing edge with no sweep ($\Lambda_{TE} = 0$ deg), and so the leading edge is swept to fit the taper ratio. The modified wing has a leading edge with no sweep ($\Lambda_{LE} = 0$ deg); thus, the trailing edge is swept to fit the same taper ratio. All other geometric parameters are unchanged. The same flow conditions are maintained except only viscous flows are used and the subsonic case will be limited to the solution with low-Mach preconditioning. The modified wing will also be different in that, because the trailing edge is now swept, grid expansion downstream of the wing will be slightly different moving from wing root to wing tip. This may have an adverse effect on the wake-based, induced-drag analysis because the wing tip is now additionally half a root chord distance farther upstream of any wake integration station relative to the wing root.

Results between the baseline wing and the modified wing for subsonic flow with preconditioning are summarized in Table 5. For the lift coefficient, both surface integration and wake integration predict a slightly lower lift value for the modified wing. This decrease in

Table 5 Comparison of lift and drag coefficients between baseline wing ($\Lambda_{TE} = 0$ deg) and modified wing ($\Lambda_{LE} = 0$ deg) for viscous, subsonic case with low-Mach preconditioning ($M_\infty = 0.25$)

Evaluation method	$\Lambda_{TE} = 0$ deg	$\Lambda_{LE} = 0$ deg
Lift: surface, Eq. (10)	0.322	0.318
Lift: wake, Eq. (11)	0.324	0.321
Drag: surface, Eq. (2)	0.0150	0.0151
Drag: wake, Eq. (12)	0.0153	0.0149
Induced	0.0046	0.0044
Total entropy (viscous)	0.0107	0.0105

Table 6 Comparison of lift and drag coefficients between baseline wing ($\Lambda_{TE} = 0$ deg) and modified wing ($\Lambda_{LE} = 0$ deg) for viscous, transonic case ($M_\infty = 0.73$)

Evaluation method	$\Lambda_{TE} = 0$ deg	$\Lambda_{LE} = 0$ deg
Lift: surface, Eq. (10)	0.413	0.405
Lift: wake, Eq. (11)	0.416	0.410
Drag: surface, Eq. (2)	0.0242	0.0255
Drag: wake, Eq. (12)	0.0246	0.0250
Induced	0.0075	0.0071
Total entropy	0.0171	0.0179
Wave	0.0055	0.0065
Viscous	0.0116	0.0114

the lift is also reflected in the slight drop in the induced drag for the modified wing. Results for the modified wing are as consistent as the baseline wing, and so the swept trailing edge apparently does not have any noticeable adverse effects on the ability to evaluate the induced drag-component.

For the transonic comparison, lift and drag coefficients are tabulated in Table 6. Again for the modified wing, the lift coefficient as predicted by both surface integration and wake integration has slightly decreased compared to the baseline wing. The induced drag, consequently, also decreases. By subtracting the wave drag from the total entropy drag, the resultant viscous drag is relatively unchanged between the two wings as expected. By isolating the shock and calculating the wave drag, the source of the major drag difference between the two wings can be ascertained.

According to surface integration, the total drag increase going from the baseline wing to the modified wing is greater than that predicted by wake integration. Unfortunately, surface integration can offer no further clarification as to why the drag increases or where the drag increase comes from. Whereas wake integration shows less difference in the total drag between the two wings, it does clearly show that the source for the drag increase can be traced to an increase in the wave drag. This increase in wave drag is the result of the stronger shock formation on the modified wing ($\Lambda_{LE} = 0$ deg) as compared to the baseline wing ($\Lambda_{LE} \approx 11$ deg).

Conclusions

The main objective of this paper is to verify the viability of using wake integration to predict the aerodynamic forces from three-dimensional flow solutions. The advantage of wake integration over the oft-used surface integration is that the former method greatly simplifies the accounting needed to extract the lift and drag from the flowfield. Although the meshes built for the case studies in this paper are all composed of a single grid wrapped around a semispan wing, this basic gridding method tends not to work for more realistic configurations such as wings with pylon-mounted engines. These configurations necessitate generating multiple grids for multiple surfaces with their inherently complex interactions. Such multiple-grid configurations pose increased bookkeeping issues for surface integration but not necessarily for wake integration.

The second advantage of wake integration is that it provides more details on the sources for drag. The general formulation for wake integration can be broken down into components that correspond to their physical sources. Such information can greatly help in minimizing drag or understanding the design tradeoffs involved between the various physical components of drag.

One significant result from this study is the apparent need to utilize low-Mach preconditioning for the inviscid subsonic case. Typically, a freestream Mach number of 0.25 does not warrant implementing a preconditioning algorithm. Convergence under this condition for a simple wing is usually not an issue, and there are no distinguishing gains in the accuracy of the lift or drag values based on surface integration. However, by looking at the drag development in the wake, significant differences can be seen. Without low-Mach preconditioning, the solution field in the wake is not fully converged to the proper state. This is reflected in the rapid dropoff in the total drag. With low-Mach preconditioning, the total drag becomes nearly constant as expected. Although preconditioning effects are more noticeable for the inviscid case, improvements can still be observed for the viscous subsonic case as well.

The viability of using wake integration was first established by studying two-dimensional flows over single-element airfoils in subsonic and transonic flows. Here results are presented for a three-dimensional flow over a NACA 0012 wing. In all cases, the lift coefficients predicted by surface integration and wake integration are in excellent agreement. For the drag coefficients, good agreements are still achieved between all integration methods. Just as important, the results prove that drag decomposition using wake integration is feasible.

The three-dimensional results obtained so far are very encouraging. Future work will involve increasing the complexity incrementally. This may entail increasing the complexity of the configuration by using multiple overset grids. These so-called Chimera grids will be initially used to cover a simple wing, but ultimately Chimera grids will be used to simulate flows about wing–body configurations. These complex cases will show how wake integration can greatly simplify the postprocessing of the flow data as well as provide more information on the physical phenomena that govern the flow problem.

References

[1]Yu, N. J., Chen, H. C., Samant, S. S., and Rubbert, P. E., "Inviscid Drag Calculations for Transonic Flows," AIAA Paper 83-1928, July 1983.

[2]Slooff, J. W., "Computational Drag Analyses and Minimization; Mission Impossible?" Drag Prediction and Minimization, AGARD-R-723, Addendum 1, 1986.

[3]van der Vooren, J., and Slooff, J. W., "CFD Based Drag Prediction; State-of-the-Art Theory, Prospects," National Aerospace Laboratory, TP 90247L, The Netherlands, Aug. 1990.

[4]Lock, R. C., "The Prediction of the Drag of Aerofoils and Wings at High Subsonic Speeds," *Aeronautical Journal*, Vol. 90, No. 896, 1986, pp. 207–226.

[5]Lock, R. C., "Prediction of the Drag of Wings at Subsonic Speeds by Viscous/Inviscid Interaction Techniques," *Drag Prediction and Minimization*, AGARD-R-723, 1986, pp. 10-1–10-71.

[6]van Dam, C. P., and Nikfetrat, K., "Accurate Prediction of Drag Using Euler Methods," *Journal of Aircraft*, Vol. 29, No. 3, 1992, pp. 516–519.

[7]van Dam, C. P., Nikfetrat, K., Wong, K., and Vijgen, P. M. H. W., "Drag Prediction at Subsonic and Transonic Speeds Using Euler Methods," *Journal of Aircraft*, Vol. 32, No. 4, 1995, pp. 839–845.

[8]Giles, M. B., and Cummings, R. M., "Wake Integration for Three-Dimensional Flowfield Computations: Theoretical Development," *Journal of Aircraft*, Vol. 36, No. 2, 1999, pp. 357–365.

[9]Hunt, D. L., Giles, M. B., and Cummings, R. M., "Wake Integration for Three-Dimensional Flowfield Computations: Application," *Journal of Aircraft*, Vol. 36, No. 2, 1999, pp. 366–373.

[10]Schmitt, V., and Destarac, D., "Recent Progress in Drag Prediction and Reduction for Civil Transport Aircraft at ONERA," AIAA Paper 98-0127, Jan. 1998.

[11]Veilleux, C., Masson, C., and Paraschivoiu, I., "A New Induced-Drag Prediction Method Using Oswatitsch's Expression," *Aeronautical Journal*, Vol. 103, No. 1024, 1999, pp. 299–307.

[12]Paparone, L., and Tognaccini, R., "Computational Fluid Dynamics–Based Drag Prediction and Decomposition," *AIAA Journal*, Vol. 41, No. 9, 2003, pp. 1647–1657.

[13]van Dam, C. P., "Recent Experience with Different Methods of Drag Prediction," *Progress in Aerospace Sciences*, Vol. 35, No. 8, 1999, pp. 751–798.

[14]Kusunose, K., Crowder, J. P., and Watzlavick, R. L., "Wave Drag Extraction from Profile Drag Based on a Wake-Integral Method," AIAA Paper 99-0275, Jan. 1999.

[15]Chao, D. D., and van Dam, C. P., "Airfoil Drag Prediction and Decomposition," *Journal of Aircraft*, Vol. 36, No. 4, 1999, pp. 675–681.

[16]Chao, D. D., "Drag Prediction and Decomposition for Airfoils and Wings," Ph.D. Dissertation, University of California, Davis, CA, March 2004.

[17]Maskell, E. C., "Progress Towards a Method for the Measurement of the Components of the Drag of a Wing of Finite Span," Royal Aircraft Establishment TR 72232, United Kingdom, 1972.

[18]Buning, P. G., Jespersen, D. C., Pulliam, T. H., Chan, W. M., Slotnick, J. P., Krist, S. E., and Renze, K. J., OVERFLOW User's Manual, Ver. 1.8, NASA, Feb. 1998.

[19]Chan, W. M., and Buning, P. G., "User's Manual for FOMOCO Utilities—Force and Moment Computation Tools for Overset Grids," NASA TM 110408, July 1996.

[20]Pulliam, T. H., and Steger, J. L., "Implicit Finite Difference Simulations of Three-Dimensional Compressible Flow," *AIAA Journal*, Vol. 18, No. 2, 1989, pp. 159–167.

[21]Spalart, P. R., and Allmaras, S. R., "A One-Equation Turbulence Model for Aerodynamic Flows," AIAA Paper 92-0439, Jan. 1992.

[22]Jespersen, D., Pulliam, T., and Buning, P., "Recent Enhancements to OVERFLOW," AIAA Paper 97-0644, Jan. 1997.